Nanoscale

RSC Publishing

PAPER

Chemistry and temperature-assisted dehydrogenation of $C_{60}H_{30}$ molecules on TiO_2(110) surfaces†

Cite this: *Nanoscale*, 2013, **5**, 11058

Carlos Sánchez-Sánchez,[ab] José Ignacio Martínez,[a] Valeria Lanzilotto,[cd] Giulio Biddau,[ef] Berta Gómez-Lor,[a] Rubén Pérez,[eg] Luca Floreano,[c] María Francisca López[a] and José Ángel Martín-Gago*[ah]

Received 18th July 2013
Accepted 31st August 2013

DOI: 10.1039/c3nr03706a

www.rsc.org/nanoscale

The thermal induced on-surface chemistry of large polycyclic aromatic hydrocarbons (PAHs) deposited on dielectric substrates is very rich and complex. We evidence temperature-assisted (cyclo)dehydrogenation reactions for $C_{60}H_{30}$ molecules and the subsequent bottom-up formation of assembled nanostructures, such as nanodomes, on the TiO_2(110) surface. To this aim we have deposited, under ultra-high vacuum, a submonolayer coverage of $C_{60}H_{30}$ and studied, by a combination of experimental techniques (STM, XPS and NEXAFS) and theoretical methods, the different chemical on-surface interaction stages induced by the increasing temperature. We show that room temperature adsorbed molecules exhibit a weak interaction and freely diffuse on the surface, as previously reported for other aromatics. Nevertheless, a slight annealing induces a transition from this (meta)stable configuration into chemisorbed molecules. This adsorbate–surface interaction deforms the $C_{60}H_{30}$ molecular structure and quenches surface diffusion. Higher annealing temperatures lead to partial dehydrogenation, in which the molecule loses some of the hydrogen atoms and LUMO levels spread in the gap inducing a net total energy gain. Further annealing, up to around 750 K, leads to complete dehydrogenation. At these temperatures the fully dehydrogenated molecules link between them in a bottom-up coupling, forming nanodomes or fullerene-like monodisperse species readily on the dielectric surface. This work opens the door to the use of on-surface chemistry to generate new bottom-up tailored structures directly on high-*K* dielectric surfaces.

Introduction

In recent years, several works have pointed out the possibility of fabricating new molecular nano-architectures, as well as two-dimensional networks, out of basic molecular precursors on metal surfaces throughout a surface-assisted (cyclo)dehydrogenation (SACDH) process.[1] SACDH has been successfully employed to synthesize new aza-fullerenes,[2,3] molecular domes,[4] and nanographenes,[5,6] from planar aromatic precursors, or even low-dimensional polyimide networks covalently interlinked from its constituent molecular building blocks.[7] However, the strong interaction of these molecular assemblies with commonly employed metallic surfaces (such as Pt, Ru, Pd, … single-crystals) heavily modifies their properties because of rehybridization. For this reason, single-crystal metallic surfaces, although greatly valuable from a fundamental point of view, do not present technological interest. Thus, one pending issue for technological applications of bottom-up assembling routes in future molecular electronics is the ability to decouple electronically the molecular nano-architectures from their supports. The same goal also applies to the search for new materials for potential photovoltaic applications. In this direction, one of the most straightforward methods could be the use of high-*K* dielectric materials as substrates due to their inertness, which, from a reactivity point of view, would enormously facilitate this goal.[8]

Unlike single-crystal metallic surfaces, where most on-surface chemistry reactions have been performed, metal oxide surfaces have been less investigated by surface science techniques due to the difficulties in obtaining long-range perfectly ordered surfaces and the chemical complexity intrinsic to the material. Amongst all metal oxides, the rutile TiO_2(110) face has

[a]*Instituto de Ciencia de Materiales de Madrid (CSIC), Sor Juana Ines de la Cruz 3, 28049 Madrid, Spain. E-mail: gago@icmm.csic.es*

[b]*EMPA, Swiss Federal Laboratories for Materials Science and Technology, Überlandstrasse 129, 8600 Dübendorf, Switzerland*

[c]*CNR-IOM, Laboratorio TASC, Basovizza SS-14, Km 163.5, I-34149 Trieste, Italy*

[d]*Department of Physics, University of Trieste, Via A. Valerio, 2 - 34127 Trieste, Italy*

[e]*Departamento de Física Teórica de la Materia Condensada, Universidad Autónoma de Madrid, 28049 Madrid, Spain*

[f]*Physics Department, Humboldt-Universität zu Berlin, Zum Grossen Windkanal 6, D-12489 Berlin, Germany*

[g]*Condensed Matter Physics Center (IFIMAC), Universidad Autonoma de Madrid, E-28049 Madrid, Spain*

[h]*Centro de Astrobiología INTA-CSIC, Torrejón de Ardoz, 28850 Madrid, Spain*

† Electronic supplementary information (ESI) available. See DOI: 10.1039/c3nr03706a

been considered as a model surface, exhibiting an intricate network of point-defects (O vacancies, Ti^{+3} states, OH adsorbates, …) and a rough topography. Thus, the electronic properties and the chemistry of the surface are history and morphology-dependent.[9] Moreover, TiO_2 is a common catalytic support, and its combination with metallic clusters leads to technologically relevant catalysts.[9] Aside from well-known catalytic metals like platinum, gold nanoparticles supported on TiO_2 have recently been revealed as highly efficient catalysts for the synthesis of aromatic compounds.[10,11] However, the intrinsic catalytic activity of TiO_2 towards molecular decomposition cannot be overlooked.[9,12] It is well-known that the reduced rutile $TiO_2(110)$-(1×1) surface includes surface-defects in the form of oxygen vacancies (O^{vac}). The formation of these vacancies leaves behind an excess of charge that partially populates the band-gap Ti-3d states, originating defective Ti^{+3} atoms.[13] This charge plays a crucial role in the catalytic properties of TiO_2 favoring dehydrogenation of small organic molecules like H_2O (see, for instance, ref. 12 and references therein).

In this contribution, we present new, clear evidence of the catalytic properties of slightly-reduced rutile TiO_2 towards on-surface (cyclo)dehydrogenation of large polycyclic aromatic hydrocarbons (PAHs). The adsorbed aromatics can be used as building blocks for the fabrication of larger nanostructures, such as fullerene-like nanodomes, by means of a temperature SACDH reaction. This work represents a further step in the search for valuable bottom-up strategies leading to the formation of new structures on more "practical" surfaces than conventional metallic single-crystals. The combination of temperature assisted on-surface chemistry with the outstanding technological capabilities of organics on TiO_2 makes this topic very promising in the search for new organic nanostructures that are suitable for improved photovoltaic cells, electronic components or the chemical industry.

Some PAHs have been recently deposited on TiO_2 surfaces, and room temperature (RT) diffusion seems to be the general rule, however, there is no information on thermally promoted chemical reactions of the as-deposited material.[8,14,15] To this goal, we have used $C_{60}H_{30}$ molecules as the PAH.[2,3] $C_{60}H_{30}$ presents a helicoidally shaped structure, whose in-vacuum optimized structure has been described in full detail elsewhere.[16] It has been previously reported that upon dehydrogenation on metal surfaces this molecule spontaneously folds into a fullerene by means of a combination of intramolecular (cyclo) dehydrogenation and dehydrogenation reactions.[2,3]

Experimental and theoretical section

Experiments have been carried out in an ultra-high vacuum chamber (UHV) with a base pressure of 1.5×10^{-10} mbar. A rutile $TiO_2(110)$ single-crystal has been prepared by consecutive sputtering and annealing (1000–1100 K) cycles under UHV conditions until a sharp LEED pattern was obtained. The cleanliness of the sample has been checked by Auger Electron Spectroscopy (AES) and STM. $C_{60}H_{30}$ molecules were synthesized following the methodology described in ref. 17 and they were evaporated in UHV using a homemade Ta crucible with a K-thermocouple spot-welded to the Ta envelope. The evaporation temperature was 650 K and the rate around 0.1 ML min^{-1}.

For the STM images, a commercial RT STM in the constant-current mode (CCT mode) was used. Images were processed with WSxM software.[18] NEXAFS and XPS experiments were carried out in the ALOISA beamline at the ELETTRA Synchrotron (Trieste, Italy). NEXAFS spectra were calibrated to the gas phase absorption spectrum of C1s in the CO molecule.[19] XPS spectra were fitted using Voigt functions, and the binding energy (BE) was calibrated using the defects peak.[20]

For *ab-initio* atomistic and molecular dynamics simulations of the different adsorbate/$TiO_2(110)$ configurations analyzed in this study, Density Functional Theory (DFT) was used effectively combining the localized-basis-set and plane-wave schemes as implemented in the FIREBALL[21] and PWSCF[22] simulation packages, respectively (see ESI†). A perturbative van der Waals (vdW) correction was used to check the reliability of the physisorbed configuration.[22] Additionally, in our STM approach, tunnelling currents for the STM images were calculated using a Keldysh–Green function formalism, together with the first-principles tight-binding Hamiltonian obtained from the local-orbital DFT-FIREBALL method (a fully detailed explanation of the methodology and structural modelling can be found in the ESI†).[21,23,24]

Results and discussion

We have deposited $C_{60}H_{30}$ molecules onto a clean $TiO_2(110)$-(1×1) surface at RT. Fig. 1(a) shows a typical STM image for approximately 0.7 ML of $C_{60}H_{30}$ grown on the $TiO_2(110)$ surface. Notwithstanding this significant coverage, also witnessed by a strong attenuation of the LEED pattern, we are not able to image molecules covering the surface in this amount. We just find some individual molecules located mainly at the step edges, since they act as nucleation sites and a few molecules fixed on terraces, probably because of their interaction with point defects of the surface. These molecules are visualized as bright triangles in good agreement with their known triangular shape when deposited on metal surfaces.[2,3,16] This shape suggests a flat, or almost flat, adsorption on the surface, which is validated by the theoretical calculations (see below). Additionally, we also observe the presence of many streaks aligned along the fast-scanning direction associated with adsorbates diffusing on the surface. This is a common behavior when organics are deposited on the $TiO_2(110)$-(1×1) surface at room temperature.[8,14,25]

The few $C_{60}H_{30}$ molecules imaged at RT on the surface exhibit a lateral size of approximately 18 Å. This value is slightly lower than the one observed when these molecules are deposited on Pt(111) (of approximately 22 Å).[2] Their apparent height is in the range of 1.7–2.5 Å depending on the bias voltage. This value is significantly higher than the 1.4 Å reported in ref. 2 for the case of Pt(111). These differences have a two-fold origin. First, a structural effect, as the interaction between $C_{60}H_{30}$ and TiO_2 is weaker than in the case of Pt, locating the molecule at a

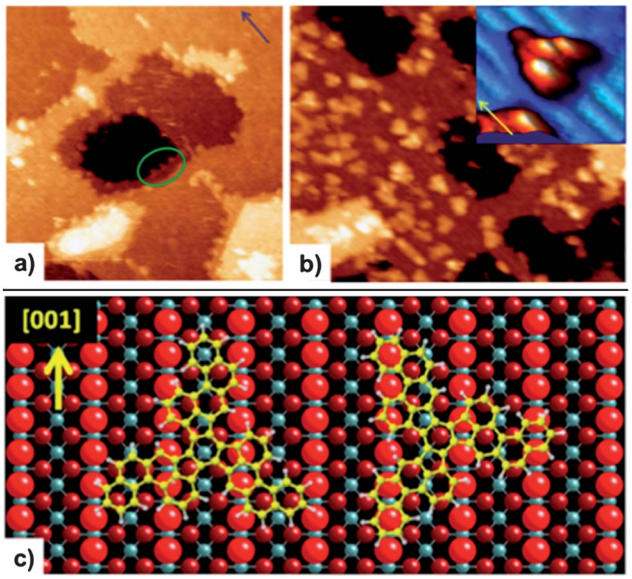

Fig. 1 Temperature induced transition from weakly bound to chemisorbed molecules. (a) STM image of the TiO_2(110)-(1×1) surface after evaporation of approximately 0.7 ML of $C_{60}H_{30}$ at RT. We observe some molecules fixed at the step edges (encircled features) and a fuzzy background, indicating molecular diffusion. Size: (500 Å × 500 Å), $I = 0.07$ nA, $V = 1.8$ V. (b) STM image after annealing (a) at around 375 K. We can see a clear increase of the "visible" material. Molecules are randomly fixed on the surface as a consequence of a change from physisorption to chemisorption. Size: (400 Å × 330 Å), $I = 0.20$ nA, $V = 1.6$ V. Inset: high-resolution STM image of a $C_{60}H_{30}$ molecule where atomic resolution on the substrate is clearly visible. (40 Å × 40 Å), $I = 0.13$ nA, $V = 1.3$ V. (c) Ball-and-stick model of the most commonly found adsorption orientations of the molecules with respect to the surface, as derived from STM images. In all images, the [001] surface direction is indicated by arrows.

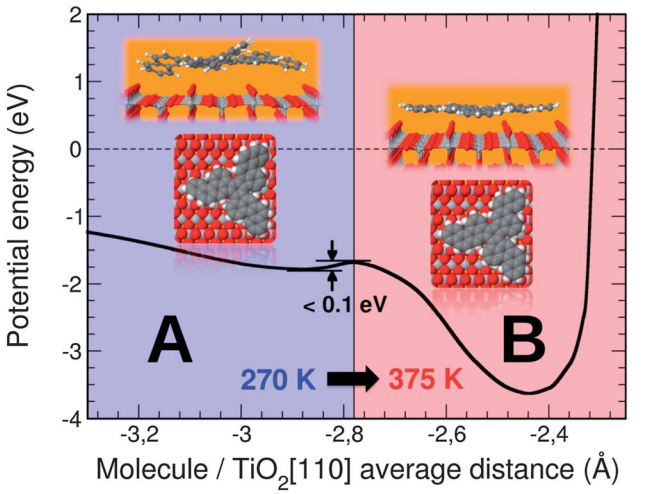

Fig. 2 Theoretical prediction of the physisorbed-like and chemisorbed $C_{60}H_{30}$/TiO_2(110) adsorption states. Pictorial representation of the potential energy (in eV) *versus* the molecule/surface average distance (in Å) for the physisorbed and chemisorbed adsorption states at temperatures of 270 and 375 K, respectively. Zero energy has been taken to be the energy corresponding to the situation with an infinite adsorbate/substrate perpendicular distance. Top- and side- ball-and-stick views of the resulting optimized configurations are shown for the physisorbed and chemisorbed interaction stages. The transition energy barrier has been determined by evaluating the difference between the experimental activation temperatures for both physisorbed-like (A) and chemisorbed (B) configurations.

higher distance from the surface. Secondly, we have an electronic effect, as the molecular orbitals are decoupled from the surface and protrude out of it. Our results point towards a weak molecule–surface interaction with molecules in a kind of physisorbed situation, which is predicted by the theoretical calculations as a weakly bounded (meta)stable on-surface state, highly resembling the $C_{60}H_{30}$ gas-phase structure (see Fig. 2(A)).

A completely different scenario is observed when the sample temperature is raised above 375 K. At this temperature, molecules are fixed on the surface, as evidenced by STM. Fig. 1(b) shows an STM image with the same molecular coverage, 0.7 ML, after annealing at 375 K the layer deposited at RT. Randomly fixed triangular features, which can be assigned to molecules, are observed. A temperature-induced molecular transformation from weakly-interacting (physisorbed) species to chemisorbed molecules has taken place. The upper inset of Fig. 1(b) shows a high-resolution STM image represented with a false-color scale to increase the contrast. It clearly shows the bright surface rows associated with five-fold Ti (Ti^{5f}) surface atoms.[26] In this image intramolecular resolution (molecular orbitals) has been attained. Examining several STM images, where atomic resolution is achieved on the substrate, two main adsorption geometries can be singled out. These are tentatively depicted in the Fig. 1(c). On the left we present the model of the preferential molecular orientation where one of the vertices of the molecule is pointing along the [001] surface direction and sitting on top of the in-plane Ti^{5f} rows. In this model, the other two molecular vertices would fall above the bridging oxygen (O^{br}) rows. On the right, we present the model for the less common case where the molecule is oriented with one of its vertices pointing along the [1–10] surface direction. In this case, the molecular side parallel to the [001] direction is sitting on top of the O^{br} rows as well as the opposite vertex. In the first case (left panel of Fig. 1(c)) we might hypothesize that the molecule tries to maximize the number of benzene rings centered on Ti^{5f} atoms, in analogy with the case of PAHs on metal surfaces.[16,17] On the opposite configuration (bottom-right panel of Fig. 1), we suggest a maximization of the number of O^{br} atoms interacting with the benzene rings.

In order to shed some light into the previously mentioned ideas, we have performed accurate DFT-based calculations effectively combining the fast and efficient localized-basis-set FIREBALL code – for molecular dynamics and geometrical optimization calculations – and the accurate plane-wave PWSCF package – for evaluating total energies – (see full details in ESI†). To obtain the $C_{60}H_{30}$ adsorption energies of both models in Fig. 1(c) we have evaluated DFT total energy differences between the whole system, and the substrate and adsorbate subsystems, with the one sketched in the bottom-left panel resulting as more stable than that shown in the bottom-right panel by around 0.4 eV per molecule. On the other hand, for the initial physisorbed-like state, detected at room temperature, DFT calculations predict an adsorption energy of 1.79 eV per molecule (see Fig. 2(A)), with the $C_{60}H_{30}$ located at an average adsorption

distance of around 2.88 Å (from the lowest peripheral atoms of the molecule to the topmost TiO_2 oxygen rows) above the TiO_2(110) surface, showing a structure closely resembling that corresponding to its gas-phase (see inset in Fig. 2(A)). The helicity of the $C_{60}H_{30}$ can be quantified by evaluating the dihedral angle between the central aromatic ring with respect to the three characteristic wings of the molecule, resulting in a value of around $\gamma = 40 \pm 2^\circ$ for all of them. This value is very close to that corresponding to the $C_{60}H_{30}$ free-molecule structure,[16] giving a clear idea about the weak interaction between the adsorbate and the substrate in this physisorbed state. Additionally, in order to improve the DFT structural and energy description of this (meta)stable adsorption configuration, we have carried out some single-point tests (given the huge size of the systems) for this configuration (and several others obtained by rigidly moving the molecule along the perpendicular-to-surface direction) by including a van der Waals (vdW) correction in a perturbative framework (implemented in PWSCF; see ESI†). The results of these additional checks reveal that the vdW contribution to the interaction is almost negligible and yields an adsorption distance and energy very similar to that obtained by conventional DFT. Thus, even though the interaction between the $C_{60}H_{30}$ and the TiO_2(110) surface is weak enough to lead to diffusion, there is a small chemical interaction linking the molecule at a relatively short adsorption distance – for a (meta)stable state – of 2.88 Å.

For the chemisorbed state, found after slight annealing up to $T = 375$ K, DFT calculations predict an adsorption energy of 3.64 eV per molecule (see Fig. 2(B)), with the $C_{60}H_{30}$ located at a shorter average adsorption distance than in the physisorbed state of around 2.44 Å from the TiO_2(110) surface. For this chemisorbed configuration, the resulting optimized structure is almost flat, just showing a slight geometrical deviation from perfect planarity due to the morphological adaptation to the topmost O^{br} rows of the substrate, and the helicity of the molecule, characteristic of the physisorbed state, disappears (see inset in Fig. 2(B)). This structural rearrangement reflects a noticeably stronger interaction in the chemisorbed regime, which can be quantified in a net adsorption energy gain of 1.85 eV per molecule with respect to the physisorbed state. As in the previous case, both models with different on-surface azimuthal orientations proposed in Fig. 1(c) have been DFT-computed for the chemisorbed state. Once again, the model proposed in the left panel yields a higher stability than the one at the right by about 0.8 eV per molecule. This observation nicely agrees with the experimental evidence of a larger abundance for the molecules displaying one vertex pointing along the [001] direction.

On the other hand, given the huge size of the adsorbate/substrate system under study, the calculation of the transition state between the physisorbed and chemisorbed configurations, as well as the simulation of the thermo-kinetic energy barrier, turn into an unfeasible task. Nevertheless, the energy barrier between both configurations can be approximately quantified by estimating the difference of temperatures at which both physi- and chemisorbed conditions are experimentally observed (270 and 375 K, respectively) and considering a transition probability at RT close to zero. This yields an approximate value slightly smaller than 0.1 eV for the energy barrier of the transition state (see Fig. 2).

Upon annealing the surface up to 750 K, the appearance of the chemisorbed molecules undergoes a strong change as seen in the STM image of Fig. 3(a). Most of the triangular-shaped $C_{60}H_{30}$ precursors become rounded and their apparent height increases (see typical structure in Fig. 3(b) and corresponding height-profile at the right side). At a first glance all the features present a similar size, and one could think that the molecules have been transformed into fullerenes, as reported for metal surfaces.[2] However, a detailed inspection of the structures shows that this is not the case. It has been shown that C_{60} fullerenes studied under same conditions present approximately a width of about 10 Å and an apparent height of 7 Å.[8] A statistical analysis of the recorded images (see ESI†) shows that the most commonly observed structures are monodisperse, about 26 ± 1.0Å wide and with heights ranging from 2.8 to 7 Å. The fact that the width of these newly formed nanostructures is much larger and the height smaller than the reported values for C_{60} molecules suggests that they have merged together into assembled molecular entities. This result evidences that at this temperature the molecule has not enough energy for a full bond rearrangement, which would lead to the formation of graphene,[1] and, therefore, some of the pentagonal bonds are preserved inside the features. The presence of pentagons within the molecular structure is responsible for the observed curvature of the nano-structures shown in Fig. 3(a) and (b), and schematically represented in Fig. 3(c). The unique way to obtain monodisperse features larger than the precursor size, like those observed in the STM images, by annealing is to follow a two-step process. Firstly, they should be partially (cyclo)dehydrogenated in their internal structure to form the inner bonds, and, secondly, they should be dehydrogenated at some of the peripheral carbon atoms, to allow the coupling between molecules into higher order fullerene-like nanodomes by on-surface addition, as evidenced in other systems.[4,27,28] Fig. 3(b) shows a

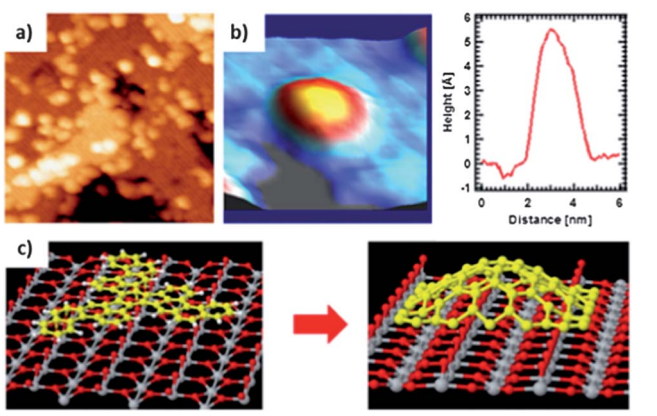

Fig. 3 (a) STM image of $C_{60}H_{30}$ precursors on the TiO_2 surface after annealing at 750 K. (300 Å × 300 Å) $I = 0.11$ nA, $V = 1.9$ V. (b) 3D representation showing a detail of one molecular nanodome. (40 Å × 40 Å) $I = 0.13$ nA, $V = 1.9$ V. A height-profile of the dome is shown on the right. (c) Ball-and-stick schematic representation of the SACDH process operating during the molecular transformation.

detail of one of the newly formed structures. Although the quality of the image might seem low due to the height of the nanostructures, atomic resolution on the Ti rows of the surface is obtained. As we can appreciate, the Figure presents clearly the characteristic round shape of the domes where only the peripheral atoms interact with the surface, while the central ones are decoupled and, consequently, topographically separated from it. Nevertheless, it is possible to find some features whose dimensions are compatible with C_{60} molecules formed upon complete dehydrogenation of the $C_{60}H_{30}$ PAH. It is important to remark that these large molecular domes are not observed when C_{60} molecules are deposited and thermally treated on the surface. This is due to the fact that in the fullerene cage there are no H atoms, which could lead to free C bonds prone to react with those of neighboring molecules. C_{60} molecules desorb from the surface after being heated at 600 K before any possible decomposition takes place, since the molecule–surface interaction is weak.[8]

In order to confirm the dehydrogenation scenario suggested by STM, we have performed spectroscopic measurements. Fig. 4(a) shows two NEXAFS spectra taken at s-polarization (*i.e.* with the electric field in the surface plane) before and after annealing at 750 K, *i.e.*, for deposited molecules and after dome formation. Two clear features can be observed, one in each spectrum. Peak A, in spectrum at 110 K, located at approximately 288.1 eV, is associated with the σ* state of the C–H bonds.[29–31] Thus, this peak indicates the existence of C–H bonds in the surface plane and, therefore, the presence of H atoms in the molecule. However, this peak vanishes (for all polarizations) after annealing the system at 750 K, indicating that the molecule is dehydrogenated at this temperature. After the annealing, a new feature in the spectrum at 750 K appears at approximately 290.5 eV (labeled as B). This new feature is associated with the π* C–O resonance on formate-like species.[32] Thus, it can be assigned to the occurrence of C–O species formed on the surface as a consequence of the interaction of dehydrogenated molecular C atoms with O atoms from the surface, probably O^{br} atoms. The observation of this feature in s-polarization is consistent with the out-of-plane curvature associated with the rim atoms of the nanodome. We have also performed XPS measurements of the C1s emission (Fig. 4(b)) for the molecules as deposited and after the dome formation. At 175 K, we can appreciate the extra core-level components associated with the different chemical environments of the C atoms (up to five different components can be distinguished), while only two remain after annealing at 750 K. These latest two components are associated with C–C bonds and C–O species, thus indicating the complete dehydrogenation of the molecule and the interaction of the peripheral C atoms with the O atoms at the surface at 750 K. We also observe a small energy shift of the high temperature C1s spectrum with respect to the one recorded at low temperature. Taking as a reference the value for the physisorbed molecule (which curiously appears at the same binding energy of that reported for a weakly interacting C_{60} overlayer[8]) the C1s core level from the domes appears shifted 0.2 eV towards lower binding energies, which could be interpreted as a small charge transfer from the substrate to the molecule induced by the chemical interaction between the molecule and surface. Thus, the newly synthesized dome structures behave as weak electron acceptors.

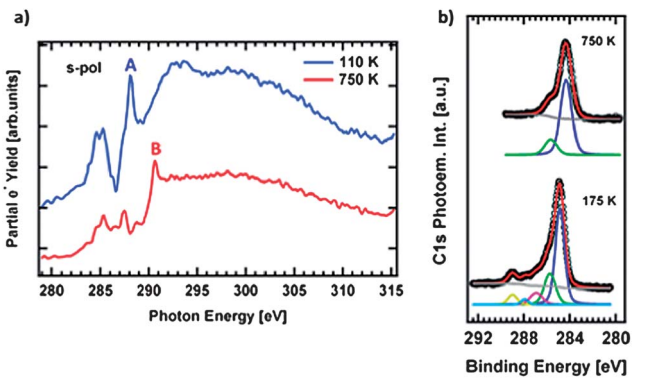

Fig. 4 Spectroscopic evidences of dehydrogenation upon annealing of the nanodomes (a) NEXAFS spectra of about 0.5 ML of $C_{60}H_{30}$ molecules deposited on TiO_2(110) recorded at s-polarization for two different temperatures, 110 K and 750 K. (b) XPS C1s photoemission core level spectra of the molecules at 175 K (physisorption state) and 750 K (complete transformation).

These data suggest that the dehydrogenation process goes through several partial steps. The C–H bonds present different energies at different molecular sites (see ESI†) and therefore it shall be cleaved at different temperatures. The first partial dehydrogenation step can be associated with the annealing at about 375 K, *i.e.*, in the regime where the molecules become chemisorbed (Fig. 1(b)). Once the molecules are stabilized on the surface, two types of molecules are observed with the STM. Some of them show a dependence of their morphological appearance on the tunneling bias while others do not change. Fig. 5(A) shows a sequence of consecutive STM images taken under the same experimental conditions, varying the tunneling bias in a large range (negative sample biases are unstable as described in ref. 8 and 9). There is a range of biases where the molecule disappears from the image (see the encircled molecules in Fig. 5(A)). This means that we are tunneling through its energy gap into the empty states of the sample with a very low density of states. Since this process is completely reversible, and the Ti rows appear unaltered through the molecule, we can disregard any molecule–tip interaction effect. The tunneling bias-dependence observed for most of the $C_{60}H_{30}$ molecules in the chemisorbed state, does not affect all of them. An example is shown in Fig. 5(B), where the molecule is unaltered after changing the bias in the same range as in the previous case. Taking into account that this different behavior is observed for molecules recorded in the same experimental session, we can disregard any preparation or tip effect. Thus, we can assign this difference to a local change of the molecular density of states driven either by a different degree of interaction with the surface or by structural modifications of the molecule. As we will see from our calculations this change of the bonding state is consistent with a partial dehydrogenation of some of the wing-most external hydrogen atoms, which can be catalyzed by the excess of charge coming on scene from the O^{vac} existing at the surface.[13]

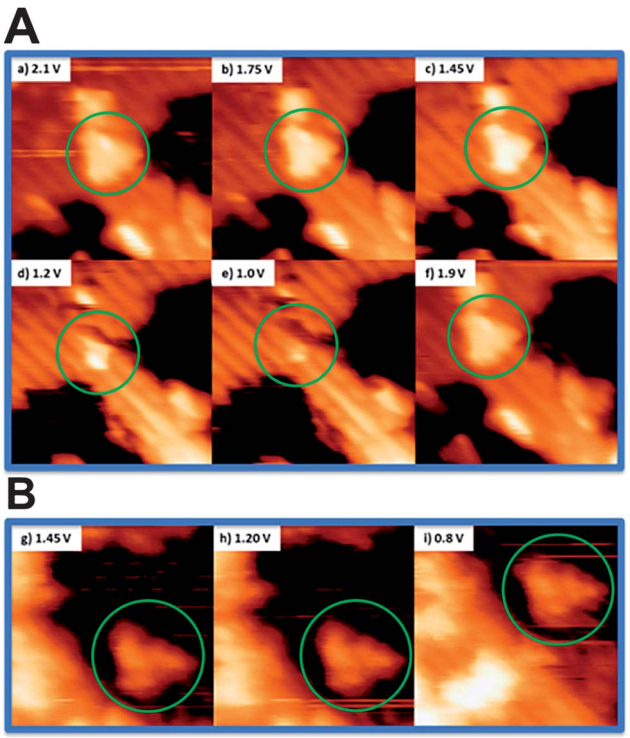

Fig. 5 Dependence of the molecular shape imaged with STM with the bias voltage. (A) Most of the imaged $C_{60}H_{30}$ molecules after annealing at 375 K disappear for low tunnelling biases. (80 Å × 80 Å), $I = 0.15$ nA. The tunnelling bias is indicated in each image. (B) The set of STM images of another molecule where no variation with the bias is observed. (50 Å × 50 Å), $I = 0.15$ nA. Tunnelling voltages are indicated in each image.

In order to understand the mechanism underlying such a surprising molecular evanescence, as well as to monitor the evolution of the electronic properties across the dehydrogenation process, we have designed a theoretical protocol by carrying out accurate DFT-based electronic structure and theoretical STM calculations (see details in ESI†). For this purpose, and based on the most preferential orientation on the $C_{60}H_{30}/TiO_2(110)$ chemisorbed configuration introduced above, we have performed full structural optimizations on the double dehydrogenated $C_{60}H_{28}/TiO_2(110)$ and the first stage of the fully dehydrogenated $C^*_{60}/TiO_2(110)$ (from now on we will denote the fully dehydrogenated $C_{60}H_{30}$ molecule as C^*_{60}, to distinguish it from the C_{60} fullerene). The geometries obtained from these processes are shown in the topmost row of Fig. 6. As we can appreciate, the double dehydrogenation of the $C_{60}H_{30}$ molecule (by removing two hydrogen atoms from a wing-edge of the molecule) produces a tendency of this wing to bond to a Ti atom of the surface, with a total energy net gain of 0.6 eV per molecule (an energy balance between the double dehydrogenation and adsorption). This effect is mostly local due to the dangling bonds appearing at the C atoms of the wing-edge after removing the two H atoms.

The left panel of Fig. 6 shows the calculated density of states profiles (projected on both the oxide surface and the molecule) for the optimized $C_{60}H_{30}/C_{60}H_{28}/C^*_{60}$ on $TiO_2(110)$ systems. In order to substantially improve the theoretical electronic characterization of the different configurations, we have used an effective "scissor operator" to align effectively the molecular and substrate energy levels according to the experimental spectroscopic data (see ESI† for more details). The result of this alignment locates the theoretical Fermi level obtained from the calculations at the experimental Ti^{+3} level (edge at 0.5 eV below the TiO_2 conduction band), and the highest occupied molecular orbital (HOMO) of the adsorbates at around 1.2 eV below this Ti^{+3} level. Once the energy levels of both adsorbate and substrate have been properly aligned and located with respect to the Ti^{+3} oxide level according to the experimental data (see ESI†), the chemisorbed $C_{60}H_{30}/TiO_2(110)$ configuration (left-top panel) reveals a band gap of about 2.3 eV, where the LUMO level is located as a broad state at around 1.3–2.2 eV above the Fermi energy. The left-middle panel of Fig. 6 shows the density of states profiles for the optimized double-dehydrogenated $C_{60}H_{28}/TiO_2(110)$ system. In this case, the broad LUMO state further spreads out by splitting into three distinct states due to the symmetry rupture. This effect favors an increase of the density of molecular states inside the gap region together with an increase of the substrate states due to the stronger interaction. The left-bottom panel of Fig. 6 shows the density of states for the first-stage of the fully dehydrogenated $C^*_{60}/TiO_2(110)$ system. Here we observe a significant narrowing of the gap with respect to the previous cases, with a wider LUMO level practically starting from the Fermi energy. Thus, the dehydrogenation process fills up the empty gap region for the $C_{60}H_x/TiO_2(110)$ system and for full dehydrogenation, the $C^*_{60}/TiO_2(110)$ case, a non-null density of states emerges at the Fermi energy. Note that the HOMO peak has not changed greatly for the dehydrogenation.

The depicted density of states, or more specifically the energy distribution of the LUMO, helps us to understand the different behavior exhibited by the molecules with the STM bias voltage. To this aim, we have calculated theoretical STM images (see ESI†) in the constant-current regime of $I = 0.2$ nA (in order to mimic the experimental conditions) for the edging cases of the chemisorbed $C_{60}H_{30}/TiO_2(110)$ and the first stage of the $C_{60}H_{28}/TiO_2(110)$. Right panel of Fig. 6 shows the STM images obtained for a tunnel bias of 1.0, 1.2 and 1.5 V for $C_{60}H_{30}/TiO_2(110)$, and of 0.8, 1.2 and 1.4 V for C_{60} $H_{28}/TiO_2(110)$ systems. Regarding the images we can observe a diffuse and small spot for 1.0 V located at the center of the molecule, whilst the LUMO level becomes visible for voltages from 1.2 V. This reproduces the experimental behavior shown in Fig. 5(A), and can be directly related to the low density of states observed up to 1.2–1.3 eV, just when the LUMO appears in the STM images. On the contrary, the LUMO remains visible whatever the positive applied tunnel bias for the $C_{60}H_{28}/TiO_2(110)$ case. This again agrees well with the experimental images shown in Fig. 5(B), and suggests that the molecules disappearing with the bias voltage are intact in the chemisorbed phase and those that are visible over the whole voltage range correspond to those that have also experienced the first step of dehydrogenation. In this case, the gap region is filled due to the narrowing of the molecule band gap, the spreading out of the LUMO level, and the induced states from the surface.

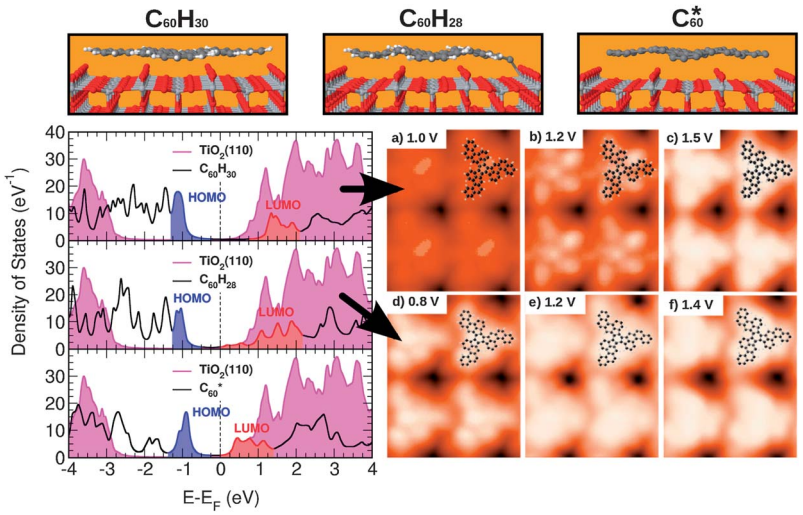

Fig. 6 Electronic and STM simulated images of $C_{60}H_{30}$ molecules with different degree of dehydrogenation. The topmost panel shows side ball-and-stick views of the resulting optimized configurations. (Left panel) Calculated density of states profiles (projected on both adsorbate and substrate) for the optimized $C_{60}H_{30}/TiO_2(110)$, $C_{60}H_{28}/TiO_2$ (110) and first stage model of the fully-dehydrogenated $C^*_{60}/TiO_2(110)$. (Right panel) Theoretical STM images for the optimized $C_{60}H_{30}/TiO_2(110)$ and $C_{60}H_{28}/TiO_2(110)$ configurations in the constant-current regime of $I = 0.2$ nA (in order to mimic the experimental scanning conditions) for same tunnel bias voltages of Fig. 5 (indicated on each STM image).

Our calculations also explain why the fully dehydrogenated molecule (C^*_{60}) cannot be converted into a fullerene (C_{60}) after all the hydrogen atoms are removed from the molecule. The relaxation process can provide a useful estimation of the first intermediate stage of the system in its fully-dehydrogenated form, just before interlinking between other dehydrogenated molecules to form the domes. In this case, after geometrical optimization, no preferential covalent bonding to the TiO_2 surface is observed, unlike the $C_{60}H_{28}$ configuration. The internal charge rearrangement after a full dehydrogenation seems to be homogeneous all over the C^*_{60} molecule, with no dangling bonds available to covalently bond to other C or to the surface, and keeping the molecule flat. Theory predicts the $C^*_{60}/TiO_2(110)$ configuration to be about 0.9 eV per molecule energetically less stable than the $C_{60}H_{28}$ case, which would permit the diffusion of the molecule on the surface. This finding agrees with the experimental information of absence of unimolecular folding into fullerenes upon dehydrogenation, and it evidences the experimentally detected thermally promoted link reaction between fully dehydrogenated molecules.[6]

Therefore, summarizing, with these experimental and theoretical results we can depict the following scenario. First of all, when $C_{60}H_{30}$ molecules are deposited on $TiO_2(110)$ at RT, they diffuse freely on the surface as all their bonds are saturated (they are not dehydrogenated molecules) and the molecule is adsorbed in a kind of weakly bound state. When the system is annealed above 375 K, $C_{60}H_{30}$ molecules chemisorb on the surface (see Fig. 1) and some of them start to undergo a partial dehydrogenation driven by the Ti^{3+} states, which anchor the molecules to the surface. Once the molecules are stabilized, we can distinguish two types of molecules according to their behavior with the tunneling bias. On the one hand, we have molecules vanishing for voltages below 1.2 V (see Fig. 5(A)). Theoretical calculations suggest that these molecules remain fully hydrogenated. These molecules present a weak interaction with the O^{br}. On the other hand, those whose STM appearance does not significantly vary with the tunneling bias (Fig. 5(B)) have suffered at least a double dehydrogenation with H atoms located at unrelated positions in the center or wings of the molecule. When this happens, the densities of state spread out into the gap region. Further annealing of the system at 750 K leads to an important molecular transformation. Individual triangular precursors convert into round fullerene-like nanodomes as a consequence of a complete cyclodehydrogenation mediated by TiO_2, as proved by NEXAFS. These nanodomes are not unimolecular, but rather formed by coalescence of different molecules linked by an addition reaction. Two or three of them usually merge to form monodisperse nanodomes, which are anchored to the O^{br} atoms. Furthermore, full dehydrogenation is associated with the chemical synthesis of new carbon allotropes, since the new C–C bonds are established between neighboring molecules to form more complex structures like fullerenes and fullerene-like nanodomes.

Conclusions

In summary, we have deeply discussed the dehydrogenation of PAHs on $TiO_2(110)$ upon thermal annealing. We have shown that a defective clean rutile $TiO_2(110)$-(1×1) surface presents catalytic activity capable of cyclodehydrogenating $C_{60}H_{30}$ when annealed at about 750 K. These activated PAHs can be used as building-blocks for the fabrication of larger nanostructures like fullerene-like nanodomes, which present different electronic properties and are decoupled from the substrate. Using TiO_2, a high-K dielectric, to induce surface chemical reactions of large organic molecules on a surface opens a new bottom-up

procedure for assembling new and valuable organic structures directly on a surface.

Acknowledgements

We acknowledge financial support by the Spanish projects MAT2011-26534, MAT2008-02929-NAN, PLE2009-0061, MAT2011-23627, CTQ2010–18813, S2009/MAT-1756/CAM and CONSOLIDER projects CDS2007-0041 and CSD2010-00024. CSS thanks the Ministerio de Educación for the AP2005-0433 FPU grant. JIM acknowledges funding from CSIC trough JaeDoc fellowship program. This research has been partially funded through the European Program "ELISA".

Notes and references

1 J. Méndez, M. F. López and J. A. Martín-Gago, *Chem. Soc. Rev.*, 2011, **40**, 4578.
2 G. G. Otero, G. Biddau, C. Sánchez-Sánchez, R. Caillard, M. F. López, C. Rogero, F. J. Palomares, N. Cabello, M. A. Basanta, J. Ortega, J. Méndez, A. M. Echavarren, R. Pérez, B. Gómez-Lor and J. A. Martín-Gago, *Nature*, 2008, **454**, 865.
3 K. Amsharov, N. Abdurakhmanova, S. Stepanow, S. Rauschenbach, M. Jansen and K. Kern, *Angew. Chem., Int. Ed.*, 2010, **49**, 9392.
4 K. T. Rim, M. Siaj, S. Xiao, M. Myers, V. D. Carpentier, L. Liu, C. Su, M. L. Steigerwald, M. S. Hybertsen, P. H. McBreen, G. W. Flynn and C. Nuckolls, *Angew. Chem., Int. Ed.*, 2007, **46**, 7891–7895.
5 M. Treier, C. A. Pignedoli, T. Laino, R. Rieger, K. Müllen, D. Passerone and R. Fasel, *Nat. Chem.*, 2010, **3**, 61.
6 A. L. Pinardi, G. Otero-Irurueta, I. Palacio, J. I. Martinez, C. Sánchez-Sánchez, M. Tello, C. Rogero, A. Cossaro, A. Preobrajenski, B. Gomez-Lor, A. Jančařík, I. G. Stará, I. Starý, M. F. López, J. Méndez and J. A. Martín-Gago, *ACS Nano*, 2013, **7**, 3676.
7 M. Treier, N. V. Richardson and R. Fasel, *J. Am. Chem. Soc.*, 2008, **130**, 14054.
8 C. Sánchez-Sánchez, V. Lanzilotto, C. González, A. Verdini, P. L. de Andrés, L. Floreano, M. F. López and J. A. Martín-Gago, *Chem.–Eur. J.*, 2012, **18**, 7382.
9 U. Diebold, *Surf. Sci. Rep.*, 2003, **48**, 53.
10 A. Corma and P. Serna, *Science*, 2006, **313**, 332.
11 A. Grirrane, A. Corma and H. García, *Science*, 2008, **322**, 1661.
12 C. L. Pang, R. Lindsay and G. Thornton, *Chem. Soc. Rev.*, 2008, **37**, 2328.
13 P. Krüger, S. Bourgeois, B. Domenichini, H. Magnan, D. Chandesris, P. Le Fevre, A. M. Flank, J. Jupille, L. Floreano, A. Cossaro, A. Verdini and A. Morgante, *Phys. Rev. Lett.*, 2008, **100**, 055501.
14 V. Lanzilotto, C. Sánchez-Sánchez, G. Bavdek, D. Cvetko, M. F. López, J. A. Martín-Gago and L. Floreano, *J. Phys. Chem. C*, 2011, **115**, 4664.
15 A. Tekiel, S. Godlewski, J. Budzioch and M. Szymonski, *Nanotechnology*, 2008, **19**, 495304.
16 G. Otero, G. Biddau, T. Ozaki, B. Gómez-Lor, J. Méndez, R. Pérez and J. A. Martín-Gago, *Chem.–Eur. J.*, 2010, **16**, 13920.
17 B. Gómez-Lor, O. de Frutos and A. M. Echavarren, *Chem. Commun.*, 1999, 2431–2432.
18 I. Horcas, R. Fernandez, J. M. Gomez-Rodriguez, J. Colchero, J. Gomez-Herrero and A. M. Baro, *Rev. Sci. Instrum.*, 2007, **78**, 013705.
19 L. Floreano, A. Cossaro, R. Gotter, A. Verdini, G. Bavdek, F. Evangelista, A. Ruocco, A. Morgante and D. Cvetko, *J. Phys. Chem. C*, 2008, **112**, 10794.
20 C. Sánchez-Sánchez, M. G. Garnier, P. Aebi, M. Blanco-Rey, P. L. de Andres, J. A. Martín-Gago and M. F. López, *Surf. Sci.*, 2013, **608**, 92.
21 J. P. Lewis, P. Jelínek, J. Ortega, A. A. Demkov, D. G. Trabada, B. Haycock, H. Wang, G. Adams, J. K. Tomfohr, E. Abad, H. Wang and D. A. Drabold, *Phys. Status Solidi B*, 2011, **248**, 1989.
22 P. Giannozzi, S. Baroni, N. Bonini, M. Calandra, R. Car, C. Cavazzoni, D. Ceresoli, G. L. Chiarotti, M. Cococcioni, I. Dabo, A. D. Corso, S. de Gironcoli, S. Fabris, G. Fratesi, R. Gebauer, U. Gerstmann, C. Gougoussis, A. Kokalj, M. Lazzeri, L. Martin-Samos, N. Marzari, F. Mauri, R. Mazzarello, S. Paolini, A. Pasquarello, L. Paulatto, C. Sbraccia, S. Scandolo, G. Sclauzero, A. P. Seitsonen, A. Smogunov, P. Umari and R. M. Wentzcovitch, *J. Phys.: Condens. Matter*, 2009, **21**, 395502.
23 J. M. Blanco, C. González, P. Jelínek, J. Ortega, F. Flores and R. Pérez, *Phys. Rev. B: Condens. Matter Mater. Phys.*, 2004, **70**, 085405.
24 J. M. Blanco, F. Flores and R. Pérez, *Prog. Surf. Sci.*, 2006, **81**, 403.
25 D. V. Potapenko, N. J. Choi and R. M. Osgood, *J. Phys. Chem. C*, 2010, **114**, 19419.
26 C. Sánchez-Sánchez, C. González, P. Jelinek, J. Méndez, P. L. de Andrés, J. A. Martín-Gago and M. F. López, *Nanotechnology*, 2010, **21**, 405702.
27 P. Lacovig, M. Pozzo, D. Alfè, P. Vilmercati, A. Baraldi and S. Lizzit, *Phys. Rev. Lett.*, 2009, **103**, 166101.
28 V. López, G. Román Pérez, A. Arregui, E. Mateo-Martí, L. Bañares, J. A. Martín-Gago, J. M. Soler, J. Gómez-Herrero and F. Zamora, *ACS Nano*, 2009, **3**, 3352.
29 J. Kikuma, K. Yoneyama, M. Nomura, T. Konishi, T. Hashimoto, R. Matsumoto, Y. Ohuchi and K. Seki, *J. Electron Spectrosc. Relat. Phenom.*, 1998, **88–91**, 919.
30 K.-H. Ernst, M. Neuber, M. Grunze and U. Ellerbeck, *J. Am. Chem. Soc.*, 2001, **123**, 493.
31 H. Oji, R. Mitsumoto, E. Ito, H. Ishii, Y. Ouchi, K. Seki, T. Yokoyama, T. Ohta and N. Kosugi, *J. Chem. Phys.*, 1998, **109**, 10409.
32 S. D. Senanayake, D. Stacchiola, J. Evans, M. Estrella, L. Barrio, M. Perez, J. Hrbek and J. A. Rodriguez, *J. Catal.*, 2010, **271**, 392.